TOF Spectrometry in Penning-Malmberg trap: analysis, calibration and investigation of signal shape

Antra Asare
Supervisors: Fredrik Parnefjord Gustafsson, Michael Doser
CERN, CH-1211, Geneva, Switzerland

Abstract

The AEgIS experiment at CERN antimatter factory is developing a technique for the capture and study of antiproton annihilation fragments in a Penning-Malmberg trap. Proof-of-principle tests were performed using low energy antiprotons (12keV) interacting with low-density buffer gas of argon and helium within the trapping region. Following annihilation, positive ions were captured and identified by ejecting them into an Microchannel Plate (MCP) detector for Time-of-Flight (TOF) spectrometry.

The objective of this summer project is to analyze TOF spectra collected during the 2023 and 2024 experimental campaigns, with the goal of extracting key calibration parameters and evaluating TOF performance indicators, such as mass resolution.

Keywords
antiprotons, TOF mass spectrometry, anti-protonic atoms, highly charged ions

1 Introduction

The AEgIS (Antimatter Experiment: Gravity, Interferometry, Spectroscopy) collaboration at CERN is dedicated to the study of fundamental interactions involving antimatter systems. AEgIS primarily focuses on producing and manipulating exotic bound systems, including antihydrogen, positonium, antiprotonic atoms, and radioactive highly charged ions (HCIs), with the overarching goal of probing fundamental symmetries and interactions [1], [5]. By synthesizing these systems and observing their spectroscopic and dynamical behavior under controlled conditions, AEgIS seeks to test the boundaries of the Standard Model and explore potential new physics.

AEgIS pioneers pulsed production of antihydrogen for tests of gravity of neutral antimatter systems. Recently, AEgIS has aimed to explore a new frontier: the capture of antiproton–nucleus annihilation fragments. These nuclear fragments are often stripped of electrons, with nucleons lost to annihilation, and are therefore typically radioactive highly charged ions.

Technologically, AEgIS relies on Penning-Malmberg traps [7], capable of manipulating both positive and negative particles through nested potential configurations. These traps operate under high magnetic fields (up to 5 T) and ultra-high vacuum conditions, which are crucial for reducing annihilation losses and ensuring long trapping times of antiprotons.

Utilizing a nested trap approach [3], ions formed from the antiproton interaction with atoms inside the trap can be studied. To analyze the products of these interactions, AEgIS employs time-of-flight (TOF) mass spectrometry. TOF spectra reveal the mass-to-charge composition of ions produced following annihilation.

This summer project involved developing an optimal noise filtering and fitting procedures for various TOF spectra, improvement of TOF calibration using electron-cooled antiproton measurements.

2 Time-of-flight mass spectrometry

In TOF mass spectrometry, the time of flight (t) is expressed according to Eq. 1 [2], [11], where L is an effective distance traveled, M is the mass of the ion, V is the accelerating voltage applied to the ion, and q is the charge of the ion. Considering that the effective voltage and the effective distance traveled is not measured directly, a calibration constant is introduced to calculate mass-to-charge ratios in helium and argon spectra presented in the upcoming publication by AEgIS collaboration. The value of the calibration constant was calculated, using the electron-cooled antiproton measurements.

$$t = L\left(\frac{M}{2Vq}\right)^{\frac{1}{2}} = C_{calib}\left(\frac{M}{q}\right)^{\frac{1}{2}} \tag{1}$$

$$C_{calib.} = \left(\frac{L^2}{2V}\right)^{\frac{1}{2}} \tag{2}$$

3 Filtering and fitting the TOF spectra

Considering that the raw data (see Fig. 1) is occasionally very noisy, methods like binning and low pass filtering are useful to prepare the data for further analysis. However, binning necessarily involves certain loss of precision, and should be therefore avoided if possible. Also, it often involves tricky decisions on the optimal bin width, which can be cumbersome, if many different datasets need to be analyzed. In this project, the data was processed via explicit Fourier filtering in Python, with various high frequency thresholds, depending on the dataset at hand.

The optimal fitting strategy for TOF signals depends strongly on the shape of the signal. For symmetric TOF distributions, a simple Gaussian fit is often sufficient [10]. However, TOF signals are frequently asymmetric, necessitating the use of asymmetric probability distributions. A commonly adopted model is the Exponentially Modified Gaussian (EMG)—a convolution of a Gaussian and an

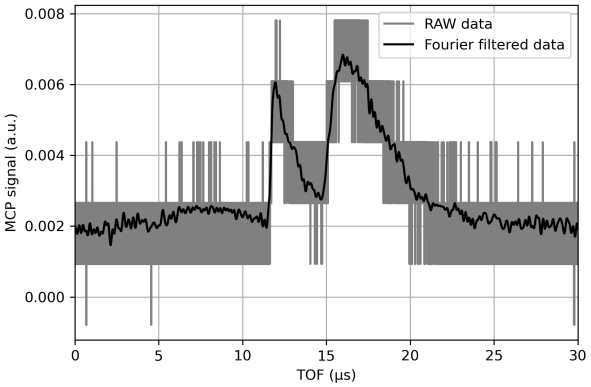

Figure 1: An example of raw data set before and after the Fourier filtering

exponential distribution—or its generalization, the hyper-EMG (hEMG), which extends the EMG by incorporating multiple exponential tails [4, 6, 9].

Currently, the most widely used approach in high-resolution TOF spectrometry is to use hyper-EMG fitting [8,9], which enables highly flexible modeling of asymmetric signal shapes. By convolving a Gaussian distribution (Eq. 3) with several exponential components, hEMG provides improved accuracy in fitting signal tails, crucial for precise mass determination. A double tailed PS-hyper-EMG distribution (Eq. 5) was used to fit antiproton spectra for calibration purposes.

$$f(x) = \frac{1}{\sigma\sqrt{2\pi}} \exp\left[-\frac{(x-x_0)^2}{2\sigma^2}\right] \tag{3}$$

$$f(x;\mu,\sigma^2,\lambda) = A\frac{\lambda}{2}\exp\left[\frac{\lambda}{2}\left(2\mu+\lambda\sigma^2-2x\right)\right]\operatorname{erfc}\left(\frac{\mu+\lambda\sigma^2-x}{\sqrt{2\sigma}}\right), \tag{4}$$

$$f(x;\mu,\sigma^2,\lambda_1,\lambda_2,\eta_1,\eta_2) = A\sum_{i=1}^{2}\eta_i\frac{\lambda_i}{2}\exp\left[\frac{\lambda_i}{2}\left(2\mu+\lambda_i\sigma^2-2x\right)\right]\operatorname{erfc}\left(\frac{\mu+\lambda_i\sigma^2-x}{\sqrt{2\sigma}}\right), \tag{5}$$

In the above equations, x is the independent variable (time in this case), and $f(x)$ denotes the corresponding probability density function (PDF). The parameter A is a normalization factor ensuring that the total integral of the distribution equals A, which can represent the total integrated signal amplitude. The parameters μ and x_0 represent the mean or centroid (TOF value) of the distribution, while σ is the standard deviation, describing the width or spread of the Gaussian core. The parameters λ, λ_1, and λ_2 are the decay rates of the exponential components that model the asymmetric tailing behavior of the TOF signals. In the hyper-EMG (hEMG) model, η_1 and η_2 are weighting coefficients (such that $\eta_1 + \eta_2 = 1$), which determine the relative contribution of each exponential tail to the total distribution. The complementary error function, $\operatorname{erfc}(\cdot)$, arises from the convolution of the Gaussian and exponential components and accounts for the asymmetric tail structure typical in experimental TOF spectra.

The full width at half maximum (FWHM) of a fitted hyper-EMG distribution was determined numerically. However, a widely adopted practical approach [4] is to estimate the mass resolution using the FWHM of the Gaussian core (Eq. 6) rather than the full hyper-EMG profile. This method is well-suited for extremely high-resolution MR-TOF analyses, where the signal shape is dominated by the Gaussian component. Nevertheless, this approximation becomes unreliable for broader, highly asymmetric peaks, where the exponential tails contribute significantly to the overall shape and thus cannot be neglected. For the purposes of this project both methods were applied. The mass resolving power was calculated as per formula 7 [8].

$$\mathrm{FWHM} = 2\sqrt{2\ln 2}\,\sigma \tag{6}$$

$$R = \frac{t_0}{2\Delta t_{\mathrm{FWHM}}} \tag{7}$$

4 Experimental data analysis

Multiple AEgIS HCI campaigns have taken place throughout 2023 and 2024 and will continue in 2025. In 2023, the first HCI TOF signal was observed due to an accidental air leak into experiment. The 2023–2024 HCI campaigns comprised several focused measurement efforts aimed at characterizing ion dynamics, trap configurations, and calibration of TOF parameters using antiprotons, electrons, and noble gases like helium and argon. Each effort sought to refine TOF spectral peak identification and trap configurations through iterative experimental setups and data fitting. Key campaigns included:

- vacuum leak checks and vacuum calibration in August 2023;
- detailed investigations of nested traps and trap floor / wall potentials in November 2023;
- helium annihilation experiment in November 2023
- argon & helium annihilation experiment to study HCI formation in August 2024
- electron-cooled antiproton trap calibration in November 2024.

4.1 $\bar{p}$ calibration runs 2024

Calibration runs with antiprotons were carried out in December 2024 and are used for the effective flight distance calibration (detailed analysis presented in the upcoming publication by AEgIS collaboration are not included in this report), and TOF mass-to-charge ratio calibration.

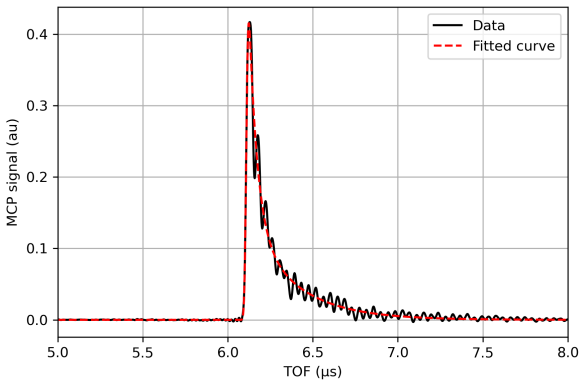

Figure 2: A sample antiproton calibration spectrum, cooling time=1, V_{wall}=190 V, V_{floor}=180 V

run_number	TOF	sigma	err_TOF	err_sigma	fwhm_num	fwhm_gaus	R_{num}	R_{gauss}
434581	6.11E-06	1.06E-08	1.62E-10	3.50E-10	7.76E-08	2.49E-08	39	123

Table 1: Antiproton calibration run results.

To find the effective distance of flight (the effective average distance between trapped ions and detector), the antiprotons were released from the trap with varied trap potential values. For each run, the TOF was estimated using hEMG fitting procedure. The square of effective distance of flight was determined by applying a linear regression model to TOF relation (Eq. 1). The estimated effective distance of flight was found to be approx. 1.1 m, which corresponds to the expected experimental value.

4.2 Helium calibration runs 2024

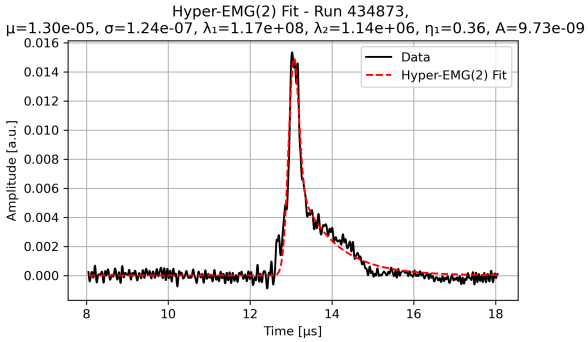

Figure 3: Helium calibration run, cooling time=70 s, V_{wall}=190 V, V_{floor}=180 V

run_number	TOF	sigma	err_TOF	err_sigma	fwhm_num	fwhm_gaus	R_{num}	R_{gauss}
434872	1.30E-05	1.19E-07	1.51E-07	1.02E-08	3.37E-07	2.81E-07	19	23
434873	1.30E-05	1.24E-07	1.40E-07	9.29E-09	3.56E-07	2.91E-07	18	22

Table 2: Helium calibration run results.

4.3 Helium runs November 2023

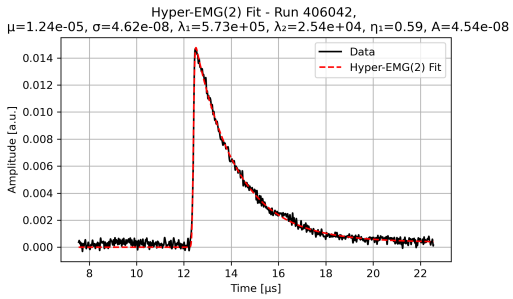

(a) Helium, cooling time = 200 s, V_{wall} = 195 V, V_{floor} = 190 V

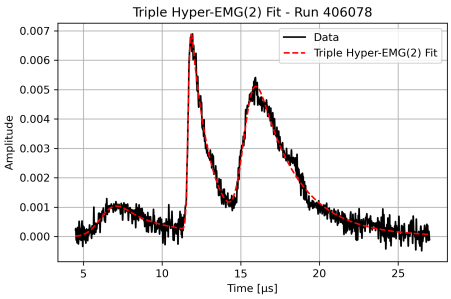

(b) H^+, He^+, He^{++}; cooling = 440 s, V_{wall} = 160 V, V_{floor} = 90 V, Catch HotStorageTime = 470 s

Figure 4: Comparison of two TOF spectra under different trap and cooling conditions.

Run (Peak)	TOF	sigma	err_TOF	err_sigma	fwhm_num	fwhm_gaus	R_{num}	R_{gauss}
406042	1.24E-05	4.62E-08	2.13E-10	2.94E-10	1.39E-06	1.09E-07	4	57
406078 (P1)	6.26E-06	7.31E-07	8.51E-08	3.23E-08	3.30E-06	1.72E-06	0.948	1.82
406078 (P2)	1.17E-05	1.11E-07	7.83E-10	9.89E-10	1.08E-06	2.61E-07	5.415	22.32
406078 (P3)	1.52E-05	5.19E-07	2.69E-09	3.30E-09	2.93E-06	1.22E-06	2.60	6.24

Table 3: Helium 2023 results.

4.4 Trap wall experiments 2024

During the course of experiments, it was observed that the level to which the trap wall is lowered upon ion release and the resulting voltage gradient does have a significant impact on TOF signal shape. Given the trap floor of 180 V, initial (closed) trap wall of 190 V, in consecutive measurements the wall was

lowered by 190 V (to zero), 150 V (to 40 V), 100 V (to 90 V), 50 V (to 140 V) and 20 V (to 170 V) (see Fig. 5). It was observed that reducing the wall to minimum level to 0 V by applying a -190 V pulse, gives the best signal in terms of peak shape, width (resolution) and signal to noise ratio.. Although, the total acceleration is the same for all setups (the total potential difference is always 180), the spatial and therefore temporal distribution of acceleration is different. When the trap wall is lower only slightly (by 20 V or 50 V) and the voltage gradient is small, the signal shape clearly displays two overlapping peaks. By increasing the release pulse and the resulting potential gradient, the signal shape converges to normal single peak hEMG.

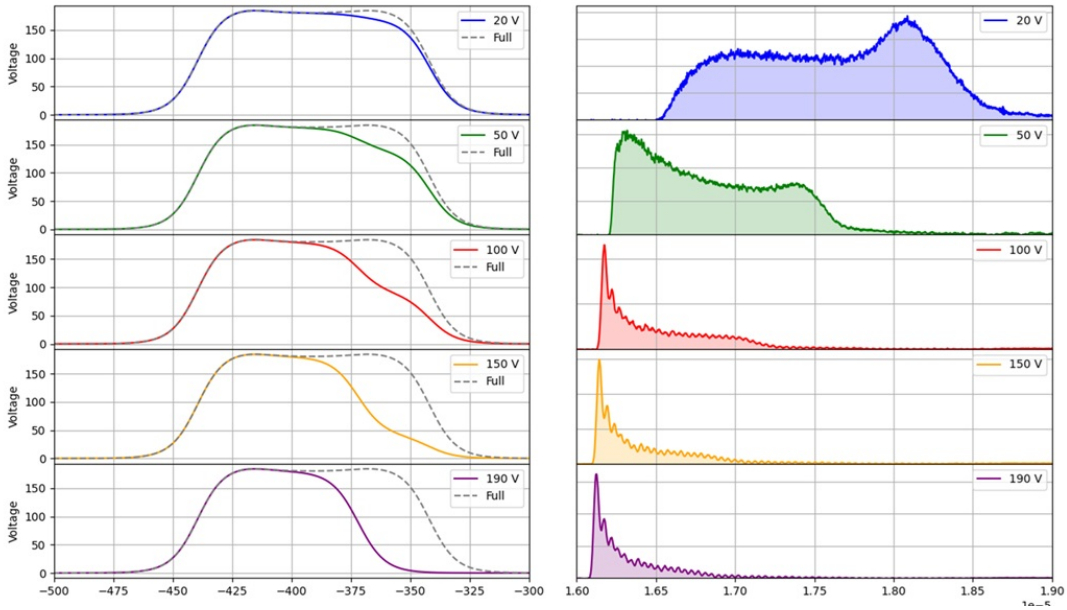

Figure 5: Left: Modeled trap potential upon release. Right: $\bar{p}$ TOF signal

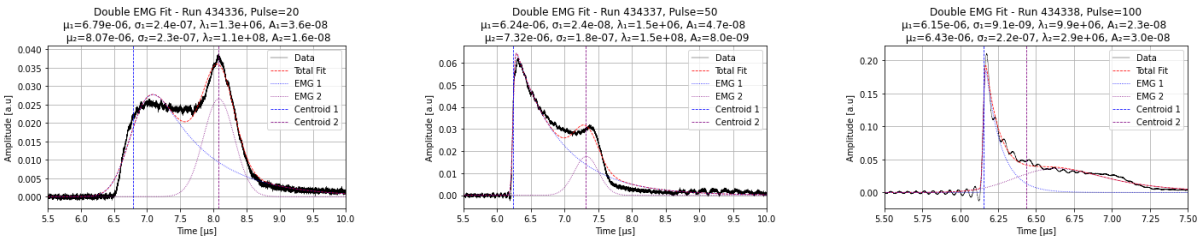

(a) Trap wall open at 170V (b) Trap wall open at 140V (c) Trap wall open at 90V

(d) Trap wall open at 40V (e) Trap wall open at 0V

Figure 6: TOF spectra and fitted TOF for trap floor of 180 V and trap wall release from 190 V with different potential release levels.

One of the tasks of this project was to fit these spectra using the sum of two EMG distributions (see Fig. 6). It may be observed that the spectra cannot be fitted satisfactory using the double peak EMG

peak structure. It appears that the underlying distribution is not EMG due to suboptimal TOF procedure. Also fitting the spectra with two peaks implies two separate species. The initial hypothesis was that the two species may be the hot and cold component of some particular ions (here antiprotons) or that the two peaks may represent the spatial distribution of ions inside the trap prior to release. A simple (without particle-particle interactions) Python simulation was created to model these two scenarios. The key variable - the steepness of potential gradient - was modeled by a Sigmoid function.

Assuming uniform spatial distribution prior to the release and the existence of two distinct temperature species (1 eV and 10 eV, because the trap is only 10 V deep) and no temperature spread whatsoever (an extreme assumption to simplify and better illustrate the point), the simulated TOF signal displays 2 peaks (see Fig. 7), when the potential gradient is very large, while there is no double peak structure when potential gradient is small. Therefore, it can be concluded that the double peak structure in antiproton experimental data (for low potential gradients) cannot be explained by the presence of separate temperature species.

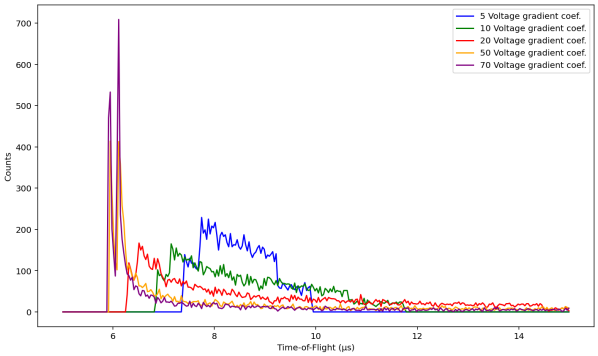

Figure 7: Simulated TOF spectrum for uniformly distributed particles of two energy species (1 eV, 10 eV) depending on the potential gradient.

Next, it was assumed that inside the trap are ions of identical energy and they are spatially distributed as shown in Fig. 8a. This assumption originates from considering just two identical charged particles inside the trap. For these initial conditions the same simulation yields a completely different result - a distinctive 2 peak structure for low potential gradients, and a convergence to one peak as the gradient increases (see Fig. 8b). This result fits the experimental results quite well (note that the energy spread is not modeled, therefore peaks don't overlap), therefore the double peak structure observed experimentally could indeed be related to the spatial distribution of ions inside the trap.

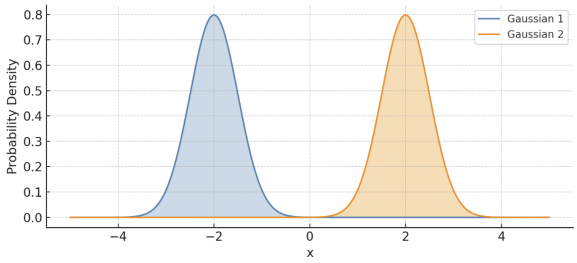

(a) Assumed spatial particle distribution inside the trap prior to release.

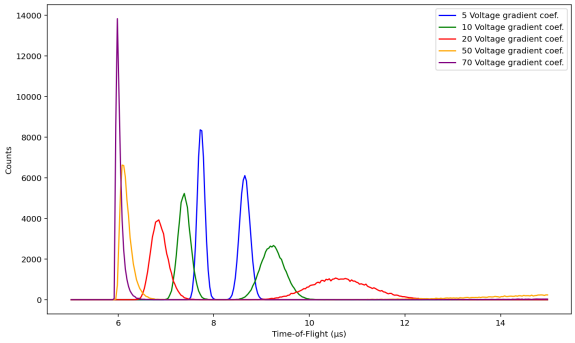

(b) Simulated TOF spectrum for non-uniformly distributed particles of single energy species depending on the potential gradient.

Figure 8: Trap distribution (left) and resulting TOF spectrum (right).

5 Conclusion

This report presented the analysis and calibration of Time-of-Flight (TOF) mass spectrometry signals from AEgIS experiments using a Penning-Malmberg trap to capture fragments from antiproton–nucleus annihilations. The project involved analyzing data of multiple campaigns carried out in 2023 and 2024.

Fourier filtering and hyper-Exponentially Modified Gaussian (hEMG) fitting was performed to accurately analyze asymmetric TOF signals. These methods enabled robust mass resolution estimations, even in the presence of noise and overlapping peaks. Calibration runs using electron-cooled antiprotons and noble gases (helium and argon) provided effective mass-to-charge scaling and confirmed an average ion flight distance of approximately 1.1 m.

Experiments on trap wall potential variation demonstrated a strong dependence of signal shape and resolution on the steepness of the voltage gradient. Simulations confirmed that the observed double-peak structures in TOF spectra are more likely due to spatial ion distributions in the trap rather than multiple thermal populations.

Bibliography

[1] Aegis collaboration - about. `https://aegis.web.cern.ch/about.php`, 2025. Accessed: 2025-07-14.

[2] Anonymous. Proceedings of the american physical society. *Phys. Rev.*, 69:674–674, Jun 1946.

[3] R Caravita. Long-term outlook for the AEgIS experimental program. Technical report, CERN, Geneva, 2025.

[4] TITAN Collaboration. Hyper-EMG: Fitting and analysis tools for hyperfine-emg lineshapes. `https://github.com/TITANCollaboration/Hyper-EMG`, 2024. Accessed: 2025-07-13.

[5] M. Doser. Antiprotonic bound systems. *Progress in Particle and Nuclear Physics*, 125:103964, 2022.

[6] Eli. Grushka. Characterization of exponentially modified gaussian peaks in chromatography. *Analytical Chemistry*, 44(11):1733–1738, 1972. PMID: 22324584.

[7] G. Kornakov, G. Cerchiari, J. Zieliński, L. Lappo, G. Sadowski, and M. Doser. Synthesis of cold and trappable fully stripped highly charged ions via antiproton-induced nuclear fragmentation in traps. *Phys. Rev. C*, 107:034314, Mar 2023.

[8] L. Nies, D. Atanasov, M. Athanasakis-Kaklamanakis, M. Au, K. Blaum, J. Dobaczewski, B. S. Hu, J. D. Holt, J. Karthein, I. Kulikov, Yu. A. Litvinov, D. Lunney, V. Manea, T. Miyagi, M. Mougeot, L. Schweikhard, A. Schwenk, K. Sieja, and F. Wienholtz. Isomeric excitation energy for $^{99}\mathrm{In}^{m}$ from mass spectrometry reveals constant trend next to doubly magic $^{100}\mathrm{Sn}$. *Phys. Rev. Lett.*, 131:022502, Jul 2023.

[9] S. Purushothaman, S. Ayet San Andrés, J. Bergmann, T. Dickel, J. Ebert, H. Geissel, C. Hornung, W.R. Plaß, C. Rappold, C. Scheidenberger, Y.K. Tanaka, and M.I. Yavor. Hyper-emg: A new probability distribution function composed of exponentially modified gaussian distributions to analyze asymmetric peak shapes in high-resolution time-of-flight mass spectrometry. *International Journal of Mass Spectrometry*, 421:245–254, 2017.

[10] R.N. Wolf, F. Wienholtz, D. Atanasov, D. Beck, K. Blaum, Ch. Borgmann, F. Herfurth, M. Kowalska, S. Kreim, Yu. A. Litvinov, D. Lunney, V. Manea, D. Neidherr, M. Rosenbusch, L. Schweikhard, J. Stanja, and K. Zuber. Isoltrap's multi-reflection time-of-flight mass separator/spectrometer. *International Journal of Mass Spectrometry*, 349-350:123–133, 2013. 100 years of Mass Spectrometry.

[11] M. M. Wolff and W. E. Stephens. A pulsed mass spectrometer with time dispersion. *Review of Scientific Instruments*, 24(8):616–617, 08 1953.